Comparison of residual stresses in sand- and chill casting of ductile cast iron wind turbine main shafts

Sonne, Mads Rostgaard; Frandsen, J. O.; Hattel, Jesper Henri

Published in:
I O P Conference Series: Materials Science and Engineering

Link to article, DOI:
10.1088/1757-899X/84/1/012025

Publication date:
2015

Document Version
Publisher's PDF, also known as Version of record

Comparison of residual stresses in sand- and chill casting of ductile cast iron wind turbine main shafts

2015 IOP Conf. Ser.: Mater. Sci. Eng. 84 012025

(http://iopscience.iop.org/1757-899X/84/1/012025)

Comparison of residual stresses in sand- and chill casting of ductile cast iron wind turbine main shafts

M R Sonne[1*], J O Frandsen[2] and J H Hattel[1]

[1]Department of Mechanical Engineering, Technical University of Denmark
[2]Global Castings A/S, Denmark

[*]Corresponding author: mrso@mek.dtu.dk

Abstract. In this work, simulations of pouring, solidification and cooling, and residual stress evolution of sand and chill cast wind turbine main shafts is performed. The models are made in the commercial software MAGMAsoft. As expected, the cooling rate of the sand casting is shown to be much lower than for the chill casting, resulting in a very course microstructure. From the simulations the nodule count is found to be 17 nodules per mm^2 and 159 nodules per mm^2 for the sand and chill casting, respectively, in the critical region of the main bearing seat. This is verified from nodule counts performed on the real cast main shafts. Residual stress evaluations show an overall increase of the maximum principal stress field for the chill casting, which is expected. However, the stresses are found to be in compression on the surface of the chill cast main shaft, which is unforeseen.

1. Introduction

The work presented in this paper is a part of a larger project called REWIND. The aim of this project is to gain knowledge for improvement of the reliability of critical wind turbine components, specifically aiming at the metallic parts in the rotor hub and the drivetrain, see Figure 1.

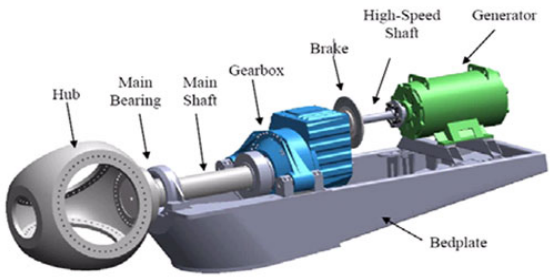

Figure 1. Schematic illustration of the main components in the nacelle of a wind turbine, showing the placement of the main shaft considered in this work.

One of the very large and critical components is the main shaft, which transfers the torque from the rotor hub into the gearbox. The main shaft is a huge cast component with a weight of approximately 12 tons. The material used for this part is ductile cast iron, which due to its spheroidal graphite has an

increased ductility compared to standard grey cast iron. The growth of these nodules is influenced by many different parameters in the manufacturing process. Of course, the ability for the inoculants, such as magnesium, to react with the oxygen and sulphur, creating MgO and MgS which floats to the surface, allows more isotropic growth. Another important factor is the cooling rate, which controls the size of the final nodules. Here, the ability of the mould to absorb the heat during solidification and cooling plays an important role. Until just recently, the main shafts for wind turbines have in industry been casted in sand moulds. But due to the low cooling rates, this process sometimes resulted in unfavourable microstructures, leading to unwanted mechanical properties and reduced reliability of the components. In order to increase the cooling rate, and thereby hopefully improve the microstructures, the main shafts can as an alternative be chill cast in permanent moulds made of ductile cast iron, which have a much higher thermal conductivity than the sand moulds. The disadvantage of using a chill for the castings is its more rigid construction and the increased thermal gradients in the casting, leading to possible higher and undesirable residual stresses in the main shafts. The aim of this paper is to address this problem by numerical simulations of the casting process. Both sand and chill casting of a specific wind turbine main shaft component will be modelled, and the residual stresses in critical regions will be compared and related to the resulting microstructures of the part. The simulations are performed in the commercial software MAGMAsoft in three subsequent steps: (i) mould filling, (ii) solidification and cooling, (iii) stress calculations. The numerical simulations are validated by comparison with real castings of the specific main shaft, which also have been performed in both sand moulds and chills.

2. Theory

The simulation of the casting processes in this work is carried out in the finite volume based commercial software MAGMAsoft [1]. The simulation consists in essence of three subsequent steps: (i) mould filling, (ii) solidification and solid state cooling, (iii) stress calculation. During mould filling, the flow field is found from solving the momentum equations and the continuity equation under the assumptions of a Newtonian fluid and incompressibility, i.e.

$$\rho \dot{u}_i + \rho\left(u_j u_{i,j}\right) = \sigma_{ij,j} + p_i + \rho g \tag{1}$$

$$\sigma_{ij} = -\delta_{ij} p + \mu(u_{i,j} + u_{j,i}) \tag{2}$$

$$u_{i,i} = 0 \tag{1}$$

which is combined with the energy equation including the convective terms, in order to obtain the temperatures during mould filling

$$\rho c_p \dot{T} + u_i\left(\rho c_p T_{,i}\right) \quad = \left(kT_{,i}\right)_{,i} + \dot{Q}''' \tag{3}$$

This is followed by the solidification analysis in which the energy equation eq (3) is solved in combination with the release of latent heat. It should be emphasized that during solidification the convective terms in eq (3) account for the natural convection taking place, and might have a considerable effect on the thermal field during solidification. However, this natural convection is neglected in the present paper in order to simplify the problem, hence reduce the calculation time. This reduces eq (3) to the heat conduction equation

$$\rho c_p \dot{T} = \left(kT_{,i}\right)_{,i} + \dot{\mathrm{Q}}''' \tag{4}$$

Kotas and Hattel [2] investigated the influence of neglecting the natural convection during solidification in large steel castings, and found that the results without convection was very similar and

showed the right tendencies compared so simulations including the convective terms during solidification.

For calculation of the transient as well as the residual stress field in the workpiece, a standard mechanical model based on the solution of the three static force equilibrium equations is used, i.e.

$$\sigma_{ij,i} + p_{,i} = 0 \tag{5}$$

Where p_i are the body forces at any point within the plate and $\sigma_{ij,i}$ is the stress tensor. The well-known Hooke's law and linear decomposition of the strain tensor as well as small strain theory are applied together with the expression for the thermal strain

$$\varepsilon_{ij}^{tot} = \varepsilon_{ij}^{el} + \varepsilon_{ij}^{pl} + \delta_{ij}\varepsilon^{th} \tag{6}$$

$$\sigma_{ij} = C_{ijkl}^{el}\varepsilon_{kl}^{el} = C_{ijkl}^{el}\left(\varepsilon_{ij}^{tot} - \varepsilon_{kl}^{pl} - \delta_{kl}\varepsilon^{th}\right) \tag{7}$$

$$C_{ijkl}^{el} = \frac{E}{1+\nu}\left[\frac{1}{2}\left(\delta_{ik}\delta_{jl} + \delta_{il}\delta_{jk}\right) + \frac{\nu}{1-2\nu}\delta_{ij}\delta_{kl}\right] \tag{8}$$

$$\varepsilon_{ij}^{tot} = \frac{1}{2}\left(u_{i,j} + u_{j,i}\right) \tag{9}$$

$$\varepsilon^{th}\left(T_1 \rightarrow T_2\right) = \int_{T_1}^{T_2} \alpha dT \tag{10}$$

The plastic strain is based on the standard J_2 flow theory with a temperature dependent von Mises yield surface. For isotropic hardening, the elastic range expands from the initial yield stress, when a load above the yield stress is applied.

$$f\left(\sigma_{ij}\right) = \frac{3}{2}s_{ij}s_{ij} = \left(\sigma_e\right)_{\max}^2 \tag{11}$$

2.1. Microstructural evolution

The microstructure of the ductile cast iron is characterized by the presence of spherical graphite particles or nodules throughout the material. These graphite nodules nucleate on small inclusions during the solidification. During eutectic solidification the graphite nodules will be surrounded by austenite, and growth of the nodules will then occur by diffusion of carbon from the liquid through the austenite shell [3]. For the final material, the graphite nodule count and size distribution are very important parameters as it influences the mechanical properties of the materials. The count of the nodules is in MAGMAsoft performed as a function of the thermal conditions according to the formulation by Oldfield [4]

$$N_A = A \cdot \Delta T^B \tag{12}$$

Where N_A is the nodule count per unit area, A is a nucleation constant and B is an exponent dependent on the effectiveness of the inoculation. ΔT is the super cooling, which is defined by the phase diagram of the considered materials composition. It is observed that the growth of the eutectic spheres is not taken into account in the microstructural model. This is a limitation of the model as both nodule count and size distribution are important for the properties of the final material [5].

3. Application

As mentioned in the introduction, the application of the numerical model is in this case the main shaft of a 3 MW wind turbine, which connects the forces from the blades on the hub, to a torque as input to the gearbox, see Figure 1. The main shafts have until now been cast in sand moulds, which as mentioned, in some cases gave unwanted microstructures (low nodule count some places in the geometry). The new development in the foundry technology is to cast the shafts in chills, which due to higher cooling rates, increases the nodule count, and hence improves the microstructural properties. The disadvantage of this process though, is an increase in residual stresses due to the higher constrains coming from the permanent mould compared to a sand mould as also mentioned in the introduction. These residual stresses can have a negative effect on the subsequent loading of the component in service (bending and torsion), but the residual stress state could also be in favour of the performance, i. e. with compressive stresses in the surface to prevent crack propagation. In the following, simulations of both sand and chill casting will be performed, and the results in terms of temperature fields, microstructure and residual stress states are compared.

3.1. Geometry and material properties

The overall dimensions of the main shaft geometry are given in Figure 2.

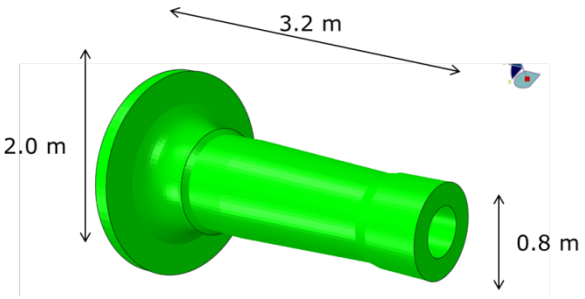

Figure 2. The overall geometry of the main shaft.

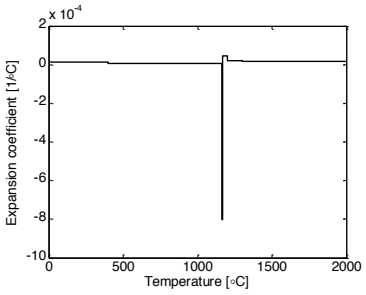

Figure 3. Thermal expansion coefficient as a function of temperature for GJS-400.

The main shafts are cast in the ductile cast iron GJS-400 with the composition as shown in Table 1.

Table 1. GJS-400 composition

C [wt.%]	Si [wt.%]	Mn [wt.%]	Mg [wt.%]	Cu [wt.%]	S [wt.%]
3.6	2.65	0.15	0.036	0.1	0.02

One of the major challenges for modelling the residual stresses in the cast component is the description of the thermal expansion component. For ductile cast irons this is special because the metal will expand during cool down due to the formation of the graphite nodules. This expansion is very much dependent on the initial inoculation, and for that reason, it can in MAGMAsoft be changed to fit if the inoculation is poor or good, and serves in this way as a fitting parameter for the simulation. It was in this work found, that with a middle inoculation, the simulations gave the best results compared to the experiment. For this setting, the temperature dependent thermal expansion is prescribed as shown in Figure 3. It is observed that the expansion coefficient is negative in the range of graphite expansion. The reason for this is how the software calculates the thermal strain, which is the change in temperature from old to new times the expansion coefficient. And as this change is negative, the thermal expansion coefficient must also be negative in order to induce a positive thermal strain.

3.2. The numerical model

The simulations are for both sand and chill casting performed according to the five steps shown in Figure 4. First pouring of melt into the mould cavity is performed, where the flow is calculated based on the Navier-Stokes equations. Then the resulting temperature field is used as initial conditions for the solidification state, where the solidification of the GJS-400 material is simulated. After solidification, the casting is further cooled down to a temperature of 400 ºC, where the casting then is shaken out of the mould, which in the numerical model is performed by removing the mould cells and prescribing a film radiation on the surface of the casting. After further cooling to a maximum temperature in the cast component of 50 ºC, the machine allowance is removed, resulting in the final geometry of the main shaft. In the numerical model this is done by "killing" the cells of the machine allowance, and recalculate the equilibrium state of stresses in the main shaft. During solidification, cooling, shake out and machining, the stress-strain analysis is performed.

Figure 4. The five steps in the simulations.

The total number of cells was chosen to be 4.000.000 in both simulation cases, with approximately 400.000 cavity cells for the fluid flow calculations. With this discretization, the calculation time was around two days on an eight cores work station. In Figure 5 and 6, the overall geometry of the two castings is shown. For the sand casting simulation (Figure 5), the filling cavity (casting and machine allowance) is surrounded by the sand drag and cope boxes modelled as cylinders, with the properties of Furan sand. For the chill casting (Figure 6), the permanent mould is modelled as one piece with the same mechanical properties as the cast material (this was also the case for the real casting). The gating system was in this case not modelled as in the real situation, since this is confidential, but the filling behavior and the overall filling time of 200 s is identical, which means that the overall temperature field after mould filling should be comparable with the temperatures in the real castings.

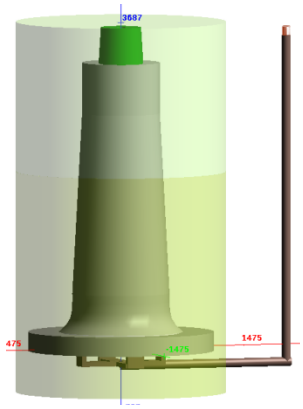

Figure 5. The overall geometry of the sand casting including the gating system.

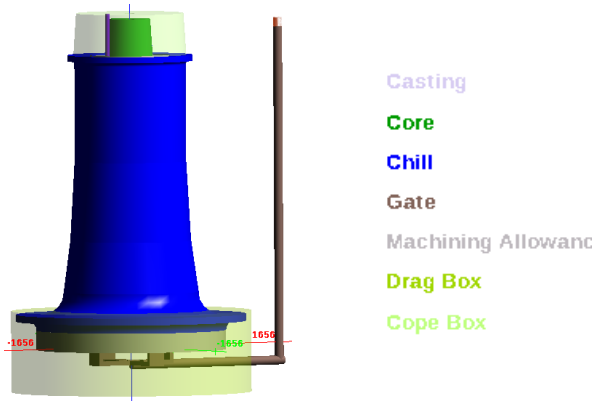

Figure 6. The overall geometry of the chill casting including the gating system

4. Results

Sand and chill casting simulations are now compared in terms of temperature history, nodule count and final residual stresses. The nodule counts were furthermore verified by comparison with the experiment, where nodule count at a critical point of the main shafts was performed by tomography.

4.1. Temperatures

In Figure 7, a contour plot of the final temperature distribution in the sand cast main shaft is shown on the cross section. The minimum temperature (blue) is 50 ^{o}C, where as it is observed that some points in the bulk material is still around 200 ^{o}C (yellow), when the calculations are stopped. In this point, the temperature history of the sand and chill castings are compared (see Figure 8 and 9). First of all it is observed, that the cooling of the sand casting takes around eight days (200 hours) compared to the one day (26 hours) of the chill casting. This was also observed for the casting experiments. In Figure 9, the temperature history during solidification in the bulk part of the main shaft is compared. It is here observed that the solidification time for the sand casting is almost five times larger than the chill casting, which of course, will have a huge effect on the resulting microstructure.

4.2. Nodule count

The modelling of the microstructure was compared with actual nodule counts performed at the main bearing seat (see Figure 10 and 11), as this is known to be a critical place for the shafts.

The nodule count was performed by tomography of which some SEM images of the sand and chill casting samples are shown in Figure 12 and 13. The volumes of the tomographic cylinders were 6.28 mm^3 and 50.24 mm^3 for the sand and chill casting, respectively, with 5 μm cut-off value for the tomography. With a sample diameter of 2 mm for the chill casting, the nodule count was calculated to be 228 nodules per mm^2. For the sand casting, the sample diameter was 4 mm and the nodule count was calculated to be 13 nodules per mm^2. This agrees very well with the values obtained in the models on Figure 10 and 11, where the nodule count is around 17 for the sand casting and 159 for the chill casting. Still, there are some deviation in the chill casting, which suggests that the cooling rate should be higher in the simulations, which could be due to a too low heat transfer coefficient between casting and mould.

Figure 7. Contour plot of the temperatures on the cross section of the main shaft, and the point where the temperature curves are extracted.

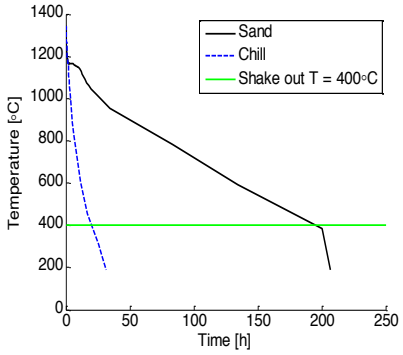

Figure 8. The overall temperature history at the point in Figure 7, for sand and chill casting, respectively.

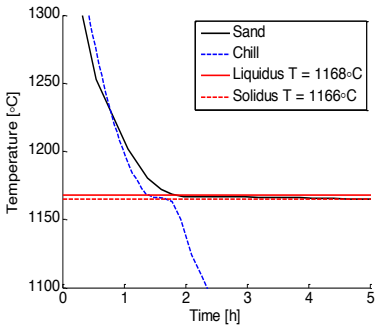

Figure 9. The temperatures during solidification at the point in Figure 7, for sand and chill casting, respectively.

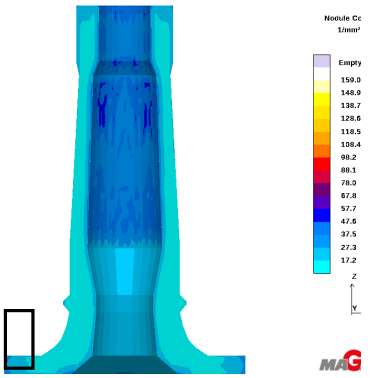

Figure 10. Nodule count per mm^2 found in the sand casting simulation. The square indicates where the nodule count was performed on the actual shaft.

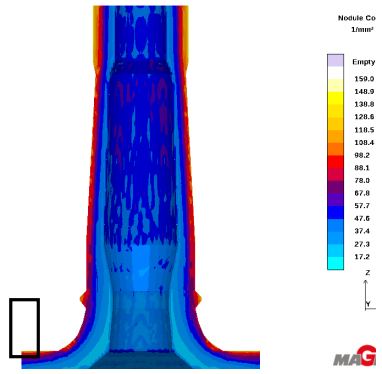

Figure 11. Nodule count per mm^2 found in the chill casting simulation. The square indicates where the nodule count was performed on the actual shaft.

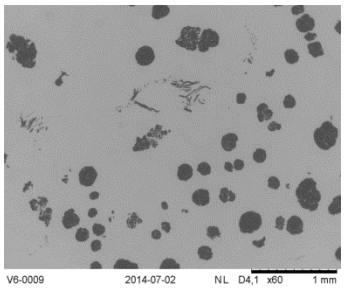

Figure 12. SEM image for the nodule count performed on the sand casting in the area shown in Figure 10.

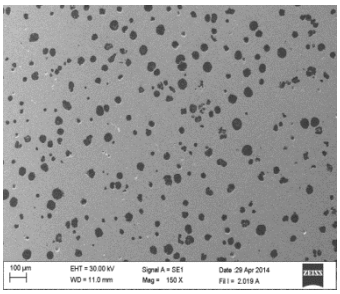

Figure 13. SEM image for the nodule count performed on the chill casting in the area shown in Figure 11.

4.3. Residual stresses

What now is interesting is to see if these enhanced micrustructures for the chill cast main shaft, has a negative effect on the corresponding residual stresses. In Figure 14 and 15, the maximum principal stress is plotted on the cross section of the sand and chill cast main shafts respectively. The stresses are normalized with respect to the yield stress due as it is confidential.

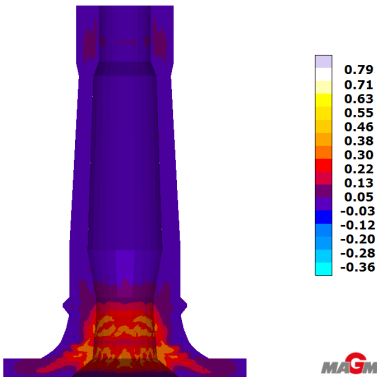

Figure 14. Maximum principal stress normalised with respect to the yield stress for the sand casting at room temperature.

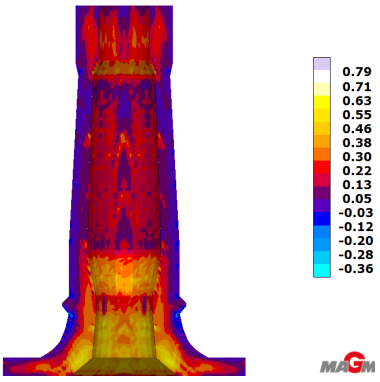

Figure 15. Maximum principal stress normalised with respect to the yield stress for the sand casting at room temperature.

It is observed that the residual stresses in the sand casted shaft are very low, with small stresses in tension on the inside of the shaft geometry. For the chill cast shaft, it is observed that the stress state in general is higher and higher tensional stresses are dominating the inside geometry of the shaft geometry. But what is an interesting finding is that the residual stresses on the outside of the shaft, which are known to be for more critical for the main shaft in-service, are in compression, which actually is beneficial for the reliability of the shaft.

5. Conclusion

Simulations of pouring, solidification and cooling and residual stress evolution of sand and chill cast wind turbine main shafts has been performed. The models were developed in the commercial software MAGMAsoft. As expected, the cooling rate of the sand casting was shown to be much lower than for the chill casting, resulting in a very course microstructure for the sand cast component. From the simulations the nodule count was found to be 17 nodules per mm^2 and 159 nodules per mm^2 for the sand and chill casting, respectively, in the critical region of the main bearing seat. This was verified from nodule counts performed on the real cast main shafts. Residual stress evaluations showed an overall increase of the maximum principal stress field for the chill casting, which was expected. But, the stresses were found to be in compression on the surface of the chill cast main shaft, which was unforeseen.

6. Acknowledgment

This work is financially supported by the Danish council for Strategic Research, which is highly acknowledged.

References

[1] ‘MAGMAsoft: v.5,2, “reference manual”, MAGMA GmbH, Aachen, Germany
[2] Kotas P and Hattel J H 2012 Modelling and simulation of A segregates: Part I, *Materials Science and Technology* **28** 872
[3] Wetterfall S-E, Fredriksson H and Hillert M. 1972 Solidification process of nodular cast iron. *J Iron Steel Inst* **210** 323
[4] Oldfield W 1966 *Trans. of the ASM* **59** 945
[5] Tanaka Y, Yang Z and Miyamoto K 1995 Evaluation of fatigue limit of spheroidal graphite cast iron *Mater Trans* **36** 749

Nomenclature

α	Thermal expansion coefficient
μ	Viscosity
ϱ	Density
v	Poisson's ratio
A	Nucleation constant
B	Inoculation exponent
c_p	Specific heat
E	Young's modulus
g	Gravitational acceleration
k	Thermal conductivity
N_A	Nodule count pr unit area
T	Temperature
ΔT	Super cooling
$\dot{Q}'''$	Volumetric heat source term
p_i	Pressure/external force vector
u_i	Velocity/displacement vector
ε_{ij}^{el}	Elastic strain tensor
ε_{ij}^{pl}	Plastic strain tensor
ε^{th}	Thermal strain
ε_{ij}^{tot}	Total strain tensor
σ_{ij}	Stress tensor
σ_e	Von-Mises equivalent stress
s_{ij}	Deviatoric stress tensor
C_{ijkl}^{el}	Elastic constitutive fourth-order tensor
$f(\sigma_{ij})$	Yield function